

We are IntechOpen, the world's leading publisher of Open Access books Built by scientists, for scientists

6,900

Open access books available

186,000

International authors and editors

200M

Downloads

Our authors are among the

154

Countries delivered to

TOP 1%

most cited scientists

12.2%

Contributors from top 500 universities



WEB OF SCIENCE™

Selection of our books indexed in the Book Citation Index
in Web of Science™ Core Collection (BKCI)

Interested in publishing with us?
Contact book.department@intechopen.com

Numbers displayed above are based on latest data collected.
For more information visit www.intechopen.com



Dual Robust Control of Grid-Connected DFIGs-Based Wind-Turbine-Systems under Unbalanced Grid Voltage Conditions

Kamel Djamel Eddine Kerrouche, Lina Wang,
Alex Van Den Bossche, Azzedine Draou,
Abdelkader Mezouar and Larbi Boumediene

Additional information is available at the end of the chapter

<http://dx.doi.org/10.5772/intechopen.75518>

Abstract

In this chapter, a comparative analysis is made for doubly-fed induction-generator (DFIG) low-voltage ride-through (LVRT) solutions. It is supposed to improve the LVRT capability of DFIG under unbalanced grid voltage conditions by hardware or software solutions. Therefore, this chapter proposes a low-cost software LVRT solution based on an efficient control scheme of DFIG driven by a wind turbine. The proposed control scheme is based on dual-sequence decomposition technique and Lyapunov-based robust control (RC) theory. Under an unbalanced grid voltage conditions, the proposed control strategy not only eliminates effectively the oscillations of the active and reactive powers exchanged between the generator and the grid but also achieves the symmetrical and sinusoidal grid currents injection. Simulation analysis under MATLAB®/Simulink® has been carried out on a 1.5 MW DFIG-based wind-turbine-systems, and the results are presented and discussed to demonstrate the feasibility and the efficiency of the control strategy for a grid-connected application under unbalanced voltage supply. The proposed dual control scheme is shown to be able to successfully mitigate torque, stator power and currents pulsations as compared with the conventional vector control based on the single control scheme.

Keywords: DFIG, LVRT, unbalanced grid voltage, robust control

1. Introduction

Variable wind turbines are known to be able to efficiently capture energy from a wide range of wind speed. Most of the variable speed wind turbines employ doubly-fed induction-generator (DFIG) due to their various advantages such as the decoupled control of the active and reactive powers, lower converter size and cost, and the feasibility of both stand-alone and grid connected operation [1, 2]. It consists of a wind turbine, gearbox, DFIG, Rotor Side Converter (RSC), Grid Side Converter (GSC) and electrical grid. In grid integration systems of DFIGs, several research studies assumed a balanced grid voltage with conventional control strategies [3]. However, in recent years, the control and operation of DFIG under disturbances and grid unbalanced have been widely studied [4]. The transient and steady-state responses of these generators during unbalanced grid voltage conditions have been presented in [5]. It has been specified from [6] that if the unbalanced grid voltage is not included in the synthesis of DFIG's controllers, high oscillations will occur in the generator torque and the injected powers might be very harmful to wind turbine components and grid connection stability. Moreover, unbalanced stator and rotor currents and DC-link voltage oscillations may lead to the increase in generator losses, temperature increase and reduction of the lifetime of DC-link capacitor [7]. Under unbalanced grid voltage, direct power control (DPC) has been adopted to control the grid-connected wind turbine-driven DFIGs in [5] by using proportional-resonant (PR) controller [7] and sliding mode control (SMC) approach [8, 9]. Moreover, in [10, 11], conventional vector control (VC). Moreover, conventional vector control (VC) with an auxiliary PI current controller has also been adopted to help regulating the negative sequence current components. Otherwise, if no negative grid voltage sequence is considered in the control loop, the occurrence of unbalanced faults can deteriorate the performance of DFIGs. Nevertheless, the control loops considered in [7, 8] keep both active and reactive power constant with reduced power ripples and at the same time significant odd order current harmonics are generated, which is not allowed by the IEEE 519-1992 [12, 13]. Therefore, an additional cost is required by active filtering [3] may not be a practicable solution for grid-connected WECS. In [14], it has been shown that during balanced or symmetrical three-phase fault, an additional STATCOM system is reported as a promising device for applications of WECS based grid-connected.

In this chapter, a review of the recently published LVRT schemes is discussed. Then, a VC approach-based dual-sequence decomposition approach associated to the Lyapunov based robust control (RC) is proposed; in order to reduce the torque ripples, minimize the active and reactive powers pulsations by obtaining sinusoidal and symmetrical injected grid currents, when the voltage at the stator is unbalanced. The details of DFIG modeling, positive and negative components separation methods and RC technique are theoretically explained in this chapter. Moreover, comprehensive simulation tests and results of the WECS are carried out and included in this chapter.

2. Wind energy generator system

In recent years, several configurations are used for the dynamic model of DFIG systems, which can be shown in various reference frames such as stationary reference frame [9] or rotating

reference frame [6, 11]. In this chapter, DFIG is modeled in a rotating reference frame under balanced and unbalanced operation conditions.

2.1. Balanced DFIG model

Using the assumption of linear magnetic circuits, the stator and rotor voltages expressions of the DFIG under balanced operating condition are written as follows [2, 15]:

$$V_s = \begin{pmatrix} v_{ds} \\ v_{qs} \end{pmatrix} = \begin{pmatrix} R_s i_{ds} + \frac{d\phi_{ds}}{dt} - \omega_s \phi_{qs} \\ R_s i_{qs} + \frac{d\phi_{qs}}{dt} + \omega_s \phi_{ds} \end{pmatrix}, V_r = \begin{pmatrix} v_{dr} \\ v_{qr} \end{pmatrix} = \begin{pmatrix} R_r i_{dr} + \frac{d\phi_{dr}}{dt} - (\omega_s - \omega) \phi_{qr} \\ R_r i_{qr} + \frac{d\phi_{qr}}{dt} + (\omega_s - \omega) \phi_{dr} \end{pmatrix} \quad (1)$$

where i_{ds} , i_{qs} , i_{dr} and i_{qr} are, respectively, the direct and quadrature stator and rotor currents. R_s and R_r are stator and rotor resistances. ω_s , ω are stator and rotor electrical angular speed, with $\omega = p \cdot \Omega_g$, p is the pair pole number. The stator and rotor fluxes can be expressed as:

$$\phi_s = \begin{pmatrix} \phi_{ds} \\ \phi_{qs} \end{pmatrix} = \begin{pmatrix} L_s i_{ds} + M i_{dr} \\ L_s i_{qs} + M i_{qr} \end{pmatrix}, \phi_r = \begin{pmatrix} \phi_{dr} \\ \phi_{qr} \end{pmatrix} = \begin{pmatrix} L_r i_{dr} + M i_{ds} \\ L_r i_{qr} + M i_{qs} \end{pmatrix} \quad (2)$$

where L_s , L_r and M are stator, rotor and mutual inductances. The active and reactive powers at the stator are defined as:

$$\begin{cases} P_s = v_{ds} i_{ds} + v_{qs} i_{qs} \\ Q_s = v_{qs} i_{ds} - v_{ds} i_{qs} \end{cases} \quad (3)$$

The principle of the conventional VC method consists of orientating the stator flux in such a way that the stator flux vector points into the d -axis direction. This approach is realized by setting the quadrature component of the stator flux to the null value:

$$\phi_s = \phi_{ds} \Rightarrow \phi_{qs} = 0 \quad (4)$$

Using the condition that the per phase stator resistance is neglected, and that the grid system is in steady state that is having a single voltage V_s that leads to stator's constant flux ϕ_s , the voltages can be easily deduced to be as:

$$\begin{cases} v_{ds} = 0 \\ v_{qs} = \omega_s \phi_s = V_s \end{cases} \quad (5)$$

The following equations are obtained when replacing the rotor flux Eq. (2) in Eq. (1) and using the above condition Eq. (5), the rotor voltages become:

$$\begin{cases} v_{dr} = \sigma L_r \frac{di_{dr}}{dt} + R_r i_{dr} - \sigma L_r \omega_r i_{qr} + \frac{M}{L_s} \frac{d\phi_{ds}}{dt} \\ v_{qr} = \sigma L_r \frac{di_{qr}}{dt} + R_r i_{qr} + \sigma L_r \omega_r i_{dr} + \omega_r \frac{M}{L_s} \phi_s \end{cases} \quad (6)$$

where V_s is the stator voltage magnitude is assumed constant, and $\omega_r = \omega_s - \omega = g\omega_s$ is the slip frequency, and g is the slip range and $\sigma = 1 - \frac{M^2}{L_s L_r}$ is the leakage coefficient. Consequently, with regard to Eq. (4), the fluxes are simplified as indicated below:

$$\begin{cases} \phi_{ds} = L_s i_{ds} + M i_{dr} \\ 0 = L_s i_{qs} + M i_{qr} \end{cases} \quad (7)$$

From Eq. (7), the stator currents can be deduced as:

$$\begin{cases} i_{ds} = \frac{\phi_{ds} - M i_{dr}}{L_s} \\ i_{qs} = -\frac{M}{L_s} i_{qr} \end{cases} \quad (8)$$

By using Eqs. (3), (5) and (8), the stator active and reactive powers can then be expressed only versus these rotor currents as:

$$\begin{cases} P_s = -V_s \frac{M}{L_s} i_{qr} \\ Q_s = -V_s \frac{M}{L_s} \left(i_{dr} - \frac{\phi_{ds}}{M} \right) \end{cases} \quad (9)$$

2.2. Unbalanced DFIG model

As stated in [10, 11], during unbalanced grid voltage, the DFIG system can be separated into positive, negative and zero sequences. In this chapter, two methods are proposed for separate positive and negative sequences: delay inverse component canceling (DICC) method. And Notch filter method.

In the first method, the components in the three-phase a, b, c system are transformed into two-phase α, β stationary reference frame. Then, the positive and negative components can be determined by the following expression:

$$\begin{pmatrix} v_{\alpha s}^+ \\ v_{\beta s}^+ \\ v_{\alpha s}^- \\ v_{\beta s}^- \end{pmatrix} = \frac{1}{2} \begin{pmatrix} 1 & 0 & 0 & -1 \\ 0 & 1 & 1 & 0 \\ 1 & 0 & 0 & 1 \\ 0 & 1 & -1 & 0 \end{pmatrix} \begin{pmatrix} v_{\alpha s}(t) \\ v_{\beta s}(t) \\ v_{\alpha s}\left(t - \frac{T}{4}\right) \\ v_{\beta s}\left(t - \frac{T}{4}\right) \end{pmatrix} \quad (10)$$

The obtained positive and negative sequences from Eq. (10) in stationary reference frame are transformed into positive and negative sequences in rotating reference frame as follows:

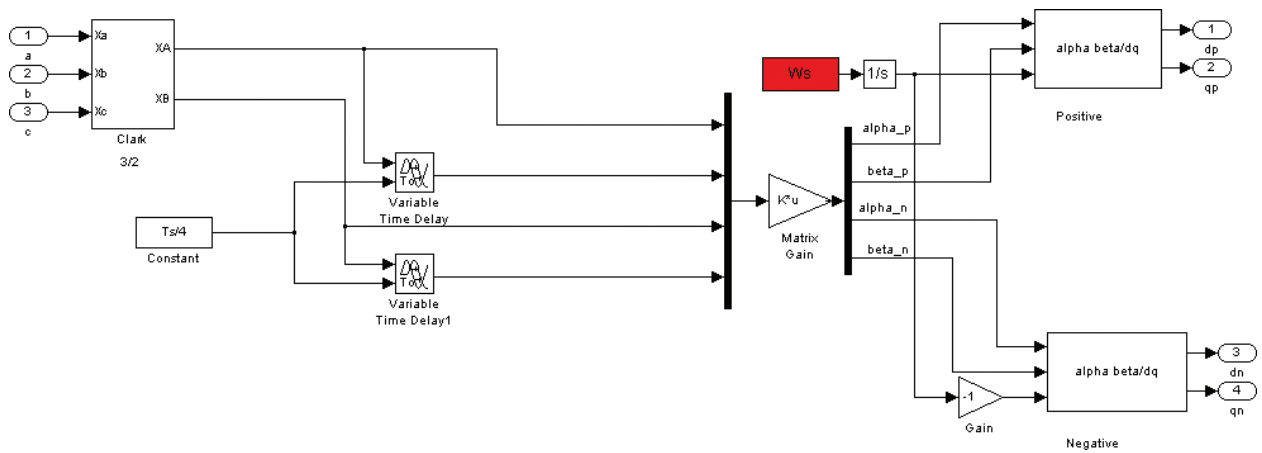


Figure 1. Simulink block for DICC method.

$$\begin{pmatrix} v_{ds}^+ \\ v_{qs}^+ \\ v_{ds}^- \\ v_{qs}^- \end{pmatrix} = \begin{pmatrix} \cos(\theta_s) & \sin(\theta_s) & 0 & 0 \\ -\sin(\theta_s) & \cos(\theta_s) & 0 & 0 \\ 0 & 0 & \cos(-\theta_s) & \sin(-\theta_s) \\ 0 & 0 & -\sin(-\theta_s) & \cos(-\theta_s) \end{pmatrix} \begin{pmatrix} v_{\alpha s}^+ \\ v_{\beta s}^+ \\ v_{\alpha s}^- \\ v_{\beta s}^- \end{pmatrix} \quad (11)$$

The associated Simulink scheme of the separate positive and negative sequences based on DICC method is depicted in Figure 1.

In the second method, the component of the negative sequence seems as a second-order harmonic in the positive rotating reference frame d, q^+ and the component of the positive sequence seems as a second-order harmonic in the negative rotating reference frame d, q^- .

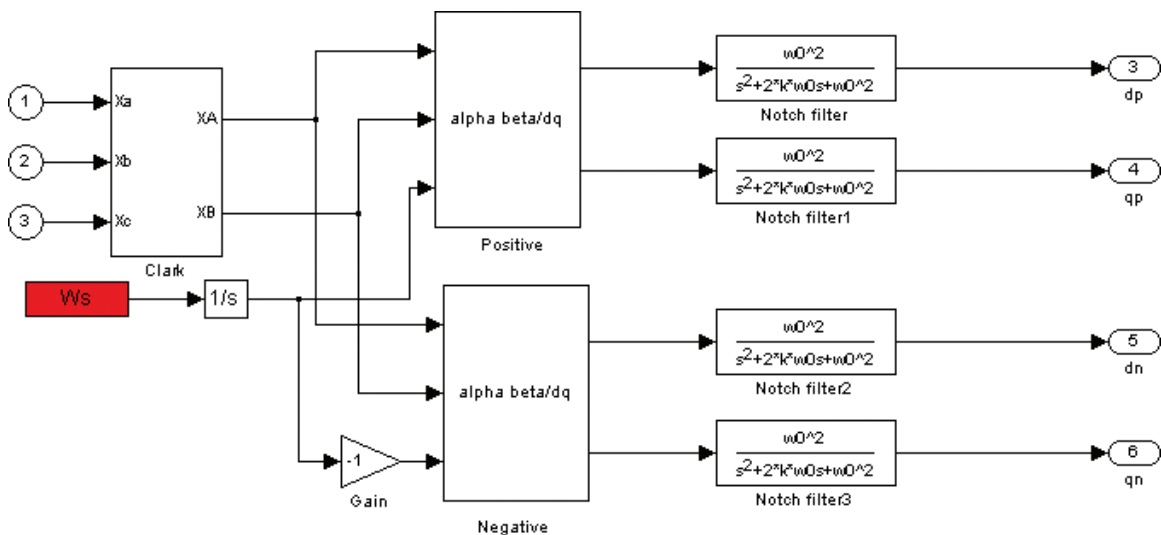


Figure 2. Simulink block for the notch filter method.

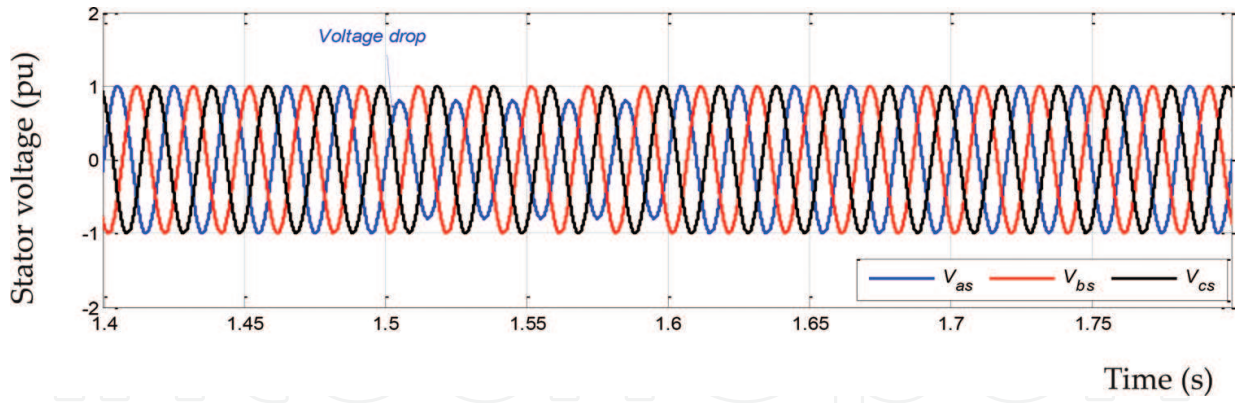


Figure 3. Grid stator voltage.

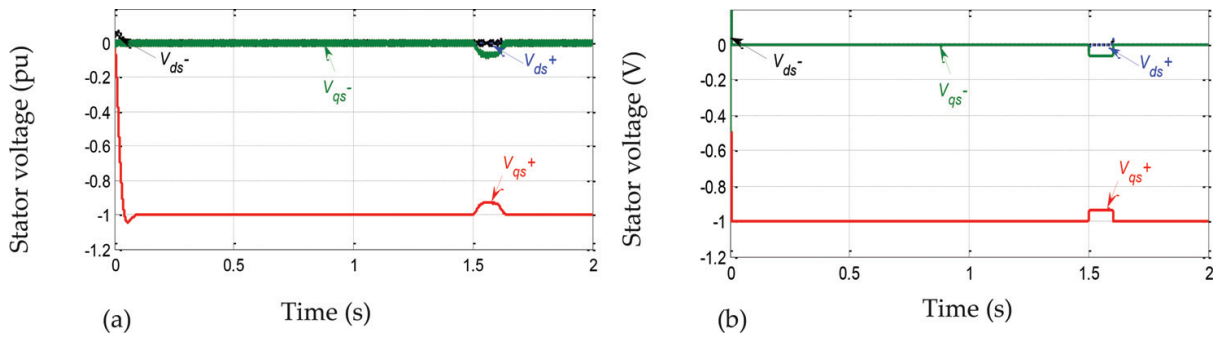


Figure 4. Unbalanced voltages in positive and negative dq rotating reference frame: (a) with DICC method and (b) with notch filter method.

Then, the DC values are bypassed and the high-frequency oscillations are suppressed by the notch filter tuned at $\omega_0 = 2\omega_s$ and $\xi = 0.707$. The associated Simulink scheme of this method is shown in **Figure 2**.

In **Figure 3**, the unsymmetrical voltage dip was applied between 1.5 and 1.6 s. Then, with two separation methods, the positive and negative sequences of the stator voltages in the rotating reference frame d, q are shown in **Figure 4**.

It can be noticed from these figures that the method based on DICC is faster than the method based on the notch filter. Therefore, the DICC method is chosen in this chapter due to its fast and precise characteristics. Assuming that the zero-sequence in the grid is neglected, the unbalanced stator voltages can be written as follows:

$$V_s^+ = \begin{pmatrix} v_{ds}^+ \\ v_{qs}^+ \end{pmatrix} = \begin{pmatrix} R_s i_{ds}^+ + \frac{d\phi_{ds}^+}{dt} - \omega_s \phi_{qs}^+ \\ R_s i_{qs}^+ + \frac{d\phi_{qs}^+}{dt} + \omega_s \phi_{ds}^+ \end{pmatrix}, V_s^- = \begin{pmatrix} v_{ds}^- \\ v_{qs}^- \end{pmatrix} = \begin{pmatrix} R_s i_{ds}^- + \frac{d\phi_{ds}^-}{dt} + \omega_s \phi_{qs}^- \\ R_s i_{qs}^- + \frac{d\phi_{qs}^-}{dt} - \omega_s \phi_{ds}^- \end{pmatrix} \quad (12)$$

The voltages at the rotor side are:

$$V_r^+ = \begin{pmatrix} v_{dr}^+ \\ v_{qr}^+ \end{pmatrix} = \begin{pmatrix} R_r i_{dr}^+ + \frac{d\phi_{dr}^+}{dt} - (\omega_s - \omega) \phi_{qr}^+ \\ R_r i_{qr}^+ + \frac{d\phi_{qr}^+}{dt} + (\omega_s - \omega) \phi_{dr}^+ \end{pmatrix}, V_r^- = \begin{pmatrix} v_{dr}^- \\ v_{qr}^- \end{pmatrix} \tag{13}$$

$$= \begin{pmatrix} R_r i_{dr}^- + \frac{d\phi_{dr}^-}{dt} - (\omega_s + \omega) \phi_{qr}^- \\ R_r i_{qr}^- + \frac{d\phi_{qr}^-}{dt} + (\omega_s + \omega) \phi_{dr}^- \end{pmatrix}$$

The stator and rotor fluxes are:

$$\begin{pmatrix} \phi_{ds}^+ \\ \phi_{qs}^+ \\ \phi_{ds}^- \\ \phi_{qs}^- \end{pmatrix} = \begin{pmatrix} L_s i_{ds}^+ + M i_{dr}^+ \\ L_s i_{qs}^+ + M i_{qr}^+ \\ L_s i_{ds}^- + M i_{dr}^- \\ L_s i_{qs}^- + M i_{qr}^- \end{pmatrix}, \begin{pmatrix} \phi_{dr}^+ \\ \phi_{qr}^+ \\ \phi_{dr}^- \\ \phi_{qr}^- \end{pmatrix} = \begin{pmatrix} L_r i_{dr}^+ + M i_{ds}^+ \\ L_r i_{qr}^+ + M i_{qs}^+ \\ L_r i_{dr}^- + M i_{ds}^- \\ L_r i_{qr}^- + M i_{qs}^- \end{pmatrix} \tag{14}$$

Under unbalanced grid, the active and reactive powers expression in Eq. (3) is decomposed into different pulsating components, which can be rewritten as:

$$\begin{pmatrix} P_s \\ Q_s \\ P_{s \sin 2} \\ P_{s \cos 2} \end{pmatrix} = \begin{pmatrix} v_{ds}^+ & v_{qs}^+ & v_{ds}^- & v_{qs}^- \\ v_{qs}^+ & -v_{ds}^+ & v_{qs}^- & -v_{ds}^- \\ v_{qs}^- & -v_{ds}^- & -v_{qs}^+ & v_{ds}^+ \\ v_{ds}^- & v_{qs}^- & v_{ds}^+ & v_{qs}^+ \end{pmatrix} \begin{pmatrix} i_{ds}^+ \\ i_{qs}^+ \\ i_{ds}^- \\ i_{qs}^- \end{pmatrix} \tag{15}$$

In order to obtain a constant stator power, the oscillating terms of the active and reactive powers $P_{s \sin 2}, Q_{s \cos 2}$ in (15) are neglected, therefore, only the average terms are controlled. By inverting (15), the stator currents can be calculated as follows:

$$\begin{pmatrix} i_{ds}^+ \\ i_{qs}^+ \\ i_{ds}^- \\ i_{qs}^- \end{pmatrix} = \frac{P_s}{D_1} \begin{pmatrix} v_{ds}^+ \\ v_{qs}^+ \\ -v_{ds}^- \\ -v_{qs}^- \end{pmatrix} + \frac{Q_s}{D_2} \begin{pmatrix} v_{qs}^+ \\ -v_{ds}^+ \\ v_{qs}^- \\ -v_{ds}^- \end{pmatrix} \tag{16}$$

where $D_1 = (v_{ds}^{+2} + v_{qs}^{+2}) - (v_{ds}^{-2} + v_{qs}^{-2})$ and $D_2 = (v_{ds}^{+2} + v_{qs}^{+2}) + (v_{ds}^{-2} + v_{qs}^{-2})$.

Figure 5 shows that the positive stator flux is aligned along with the d^+ -axis and rotates at the speed of ω_s , whereas the d^- -axis rotates at an angular speed of $-\omega_s$, with the phase angle to the α -axis being $-\theta_s$. Therefore, by using Eq. (12) with stator flux orientation under unbalanced grid, the stator currents are simplified as follows:

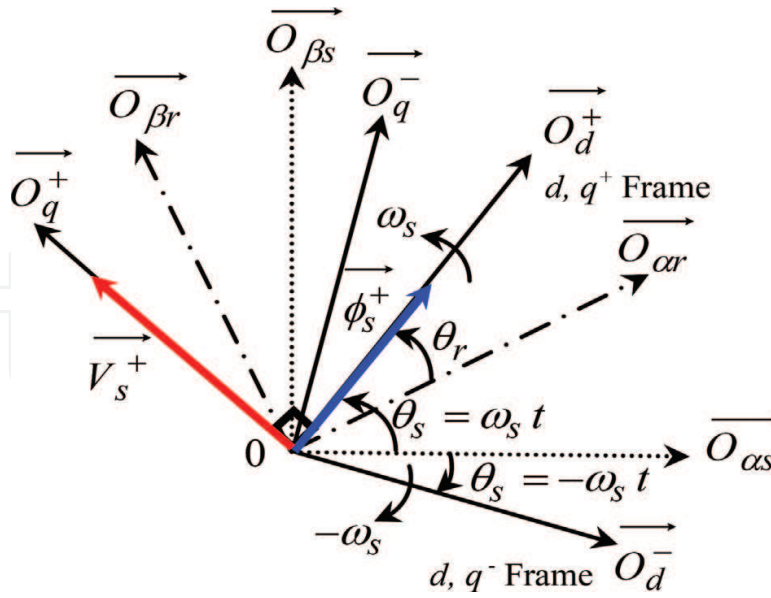


Figure 5. Stator flux orientation under unbalanced grid.

$$\begin{pmatrix} i_{ds}^+ \\ i_{qs}^+ \\ i_{ds}^- \\ i_{qs}^- \end{pmatrix} = \frac{1}{L_s} \begin{pmatrix} \phi_{ds}^+ \\ 0 \\ \phi_{ds}^- \\ 0 \end{pmatrix} - \frac{M}{L_s} \begin{pmatrix} i_{dr}^+ \\ i_{qr}^+ \\ i_{dr}^- \\ i_{qr}^- \end{pmatrix} \tag{17}$$

Combining Eq. (17) with Eq. (16), the rotor currents are written as follows:

$$\begin{pmatrix} i_{dr}^+ \\ i_{qr}^+ \\ i_{dr}^- \\ i_{qr}^- \end{pmatrix} = -\frac{L_s P_s}{M D_1} \begin{pmatrix} v_{ds}^+ \\ v_{qs}^+ \\ -v_{ds}^- \\ -v_{qs}^- \end{pmatrix} - \frac{L_s Q_s}{M D_2} \begin{pmatrix} v_{qs}^+ \\ -v_{ds}^+ \\ v_{qs}^- \\ -v_{ds}^- \end{pmatrix} + M \begin{pmatrix} \phi_{ds}^+ \\ 0 \\ \phi_{ds}^- \\ 0 \end{pmatrix} \tag{18}$$

3. Controllers design

The details of the conventional Lyapunov-based robust control have been presented in [16–18], so, this control strategy with unbalanced DFIG model is considered in this chapter.

3.1. Tracking error

In this chapter, J. J. Slotine [16] proposed the used tracking error:

$$S(x) = \left(\frac{\partial}{\partial t} + \lambda_x \right)^{n-1} e(x) \tag{19}$$

where $e(x)$ is the error vector ($e(x) = x^* - x$), λ_x is a positive coefficient, n is the system order. To bring the state variable to the tracking errors, the following two conditions have to be satisfied:

$$S(x) = 0, \quad \frac{d}{dt}S(x) = 0 \tag{20}$$

For $n = 1$ in Eq. (19), the errors of direct and quadrature rotor currents are chosen as:

$$S(x) = \begin{cases} S_1(i_{dr}^+) = i_{dr}^{+*} - i_{dr}^+ \\ S_2(i_{qr}^+) = i_{qr}^{+*} - i_{qr}^+ \\ S_3(i_{dr}^-) = i_{dr}^{-*} - i_{dr}^- \\ S_4(i_{qr}^-) = i_{qr}^{-*} - i_{qr}^- \end{cases} \tag{21}$$

3.2. Control law

In this chapter, the Lyapunov-based robust control is used to generate voltage references as an input to PWM. The control law satisfies the previous conditions is presented in the following form:

$$V_r = V_{r,eq} + V_{r,n} \tag{22}$$

where V_r is the control vector, $V_{r,eq}$ is the equivalent control vector, $V_{r,n}$ is the switching part of the control law.

The derivative of the tracking error (20) is rewritten as follows:

$$\frac{d}{dt}S(x) = F + D V_r \tag{23}$$

From Eq. (20), when the trajectories of rotor currents converge toward their references, the derivative of the tracking error is:

$$\frac{d}{dt}S(x) = F + D V_r = 0 \tag{24}$$

The following equation is obtained by replacing the rotor flux Eq. (14) in Eqs. (12) and (13) and combining with Eq. (24):

$$F = \begin{bmatrix} F_1 \\ F_2 \\ F_3 \\ F_4 \end{bmatrix} = \begin{bmatrix} i_{dr}^{+*} + \frac{R_r}{\sigma L_r} i_{dr}^+ - \omega_r i_{qr}^+ + \frac{M}{\sigma L_r L_s} v_{ds}^+ \\ \frac{R_r}{\sigma L_r} i_{qr}^+ + \dot{i}_{qr}^{+*} + \omega_r i_{dr}^+ + \frac{M}{\sigma L_r L_s} v_{qs}^+ \\ -\frac{M}{\sigma L_r L_s} \phi_{sd}^+ (\omega_s - \omega_r) \\ i_{dr}^{-*} + \frac{R_r}{\sigma L_r} i_{dr}^- - \omega_r i_{qr}^- + \frac{M}{\sigma L_r L_s} v_{ds}^- \\ \frac{R_r}{\sigma L_r} i_{qr}^- + \dot{i}_{qr}^{-*} + \omega_r i_{dr}^- + \frac{M}{\sigma L_r L_s} v_{qs}^- \\ -\frac{M}{\sigma L_r L_s} \phi_{sd}^- (\omega_s + \omega_r) \end{bmatrix} \tag{25}$$

where

$$D = \frac{1}{\sigma L_r} \begin{bmatrix} 1 & 0 & 0 & 0 \\ 0 & 1 & 0 & 0 \\ 0 & 0 & 1 & 0 \\ 0 & 0 & 0 & 1 \end{bmatrix} \quad (26)$$

The following control law is obtained:

$$V_r = -D^{-1} \begin{bmatrix} F_1 + K_1 \text{sat}(S_1) \\ F_2 + K_2 \text{sat}(S_2) \\ F_3 + K_3 \text{sat}(S_3) \\ F_4 + K_4 \text{sat}(S_4) \end{bmatrix} \quad (27)$$

and

$$\text{sat}(S_i) = \begin{cases} 1, & S_i > \lambda_i \\ S_i/\lambda_i, & |S_i| \leq \lambda_i \\ -1, & S_i < -\lambda_i \end{cases} \quad (28)$$

where λ_i is the width boundary layer and i indicates 1, 2, 3 or 4 and K_1, K_2, K_3 and K_4 are positive control gains of the switching control part.

3.3. Lyapunov stability proof

The stability and robustness of the system are thoroughly investigated and subsequent results are presented in [16–18]. In this chapter, the stability theory of Lyapunov is used to check the convergence of the tracking errors toward the zero by satisfying the following condition:

$$\dot{V} = S^T(x) \dot{S}(x) \leq 0 \quad (29)$$

Then, the Lyapunov function is obtained as:

$$\dot{V} = S^T(x) (F + D V_r) \leq 0 \quad (30)$$

By using Eq. (27), Lyapunov function Eq. (30) is rewritten as:

$$\dot{V} = S^T(x) \left(F + D \left(-D^{-1} \begin{bmatrix} F_1 + K_1 \text{sat}(S_1) \\ F_2 + K_2 \text{sat}(S_2) \\ F_3 + K_3 \text{sat}(S_3) \\ F_4 + K_4 \text{sat}(S_4) \end{bmatrix} \right) \right) \leq 0 \quad (31)$$

Or

$$\dot{V} = -S^T(x) \begin{bmatrix} K_1 \text{sat}(S_1) \\ K_2 \text{sat}(S_2) \\ K_3 \text{sat}(S_3) \\ K_4 \text{sat}(S_4) \end{bmatrix} \leq 0 \quad (32)$$

From Eq. (32), the Lyapunov function is definitely negative so that the control law becomes stable.

3.4. Lyapunov robustness proof

In practice, the tracking error S will be influenced by the parameter variations and measurement uncertainties. Thus, Eq. (23) is rewritten as:

$$\frac{d}{dt} S(x) = F + D V_r + H \quad (33)$$

where $H = [H1 \ H2 \ H3 \ H4]^T$ represents system disturbances. Thus, Eq. (35) can be rewritten as:

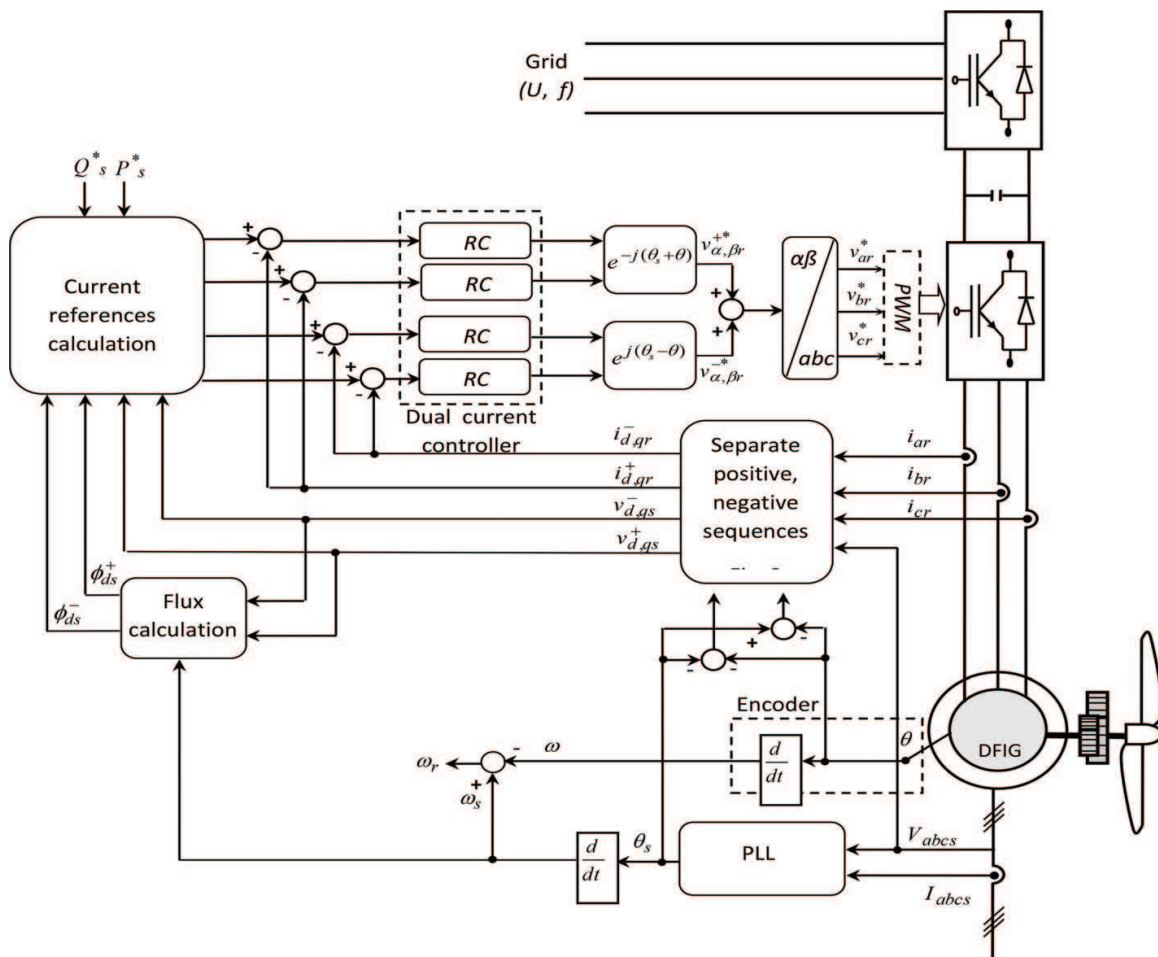


Figure 6. Block diagram of the proposed Lyapunov-based robust control scheme.

$$\dot{V} = S^T(x) \begin{pmatrix} H_1 \\ H_2 \\ H_3 \\ H_4 \end{pmatrix} - \begin{bmatrix} K_1 \text{sat}(S_1) \\ K_2 \text{sat}(S_2) \\ K_3 \text{sat}(S_3) \\ K_4 \text{sat}(S_4) \end{bmatrix} \leq 0 \quad (34)$$

It is worth mentioning that if the positive control gains satisfy the following condition, specifically, $K_1 > |H_1|$, $K_2 > |H_2|$, $K_3 > |H_3|$ and $K_4 > |H_4|$ the time derivative of Lyapunov function \dot{V} is still definitely negative. Consequently, the control law features are robust. **Figure 6** shows the block diagram of the VC scheme for DFIG using Lyapunov-based robust control (RC). In this block diagram, the Phase-Locked-Loop (PLL) estimates the frequency, the grid voltage magnitude and the stator angle. The block of separate positive and negative sequences of the current and the voltage shown in **Figure 1** is used in this schema for the dual current controller and the calculation of the current references.

4. Simulation results

The generator is tested under single line to ground fault condition on phase 'a'; at 1.5 s an unbalanced voltage drop of 20% is created for a time of 0.1 s as shown in **Figure 3**. In this section, all the physical quantities are in per unit values, and the quantities of the rotor are referred to the stator side. **Figure 7** shows the Simulink block diagram of the DFIG wind turbine model. The switching frequency of converter is set to 1 kHz; the nominal DC converter is set to 2000 V. Wind speed varies from 10 to 11 m/s. To examine the validity of the proposed

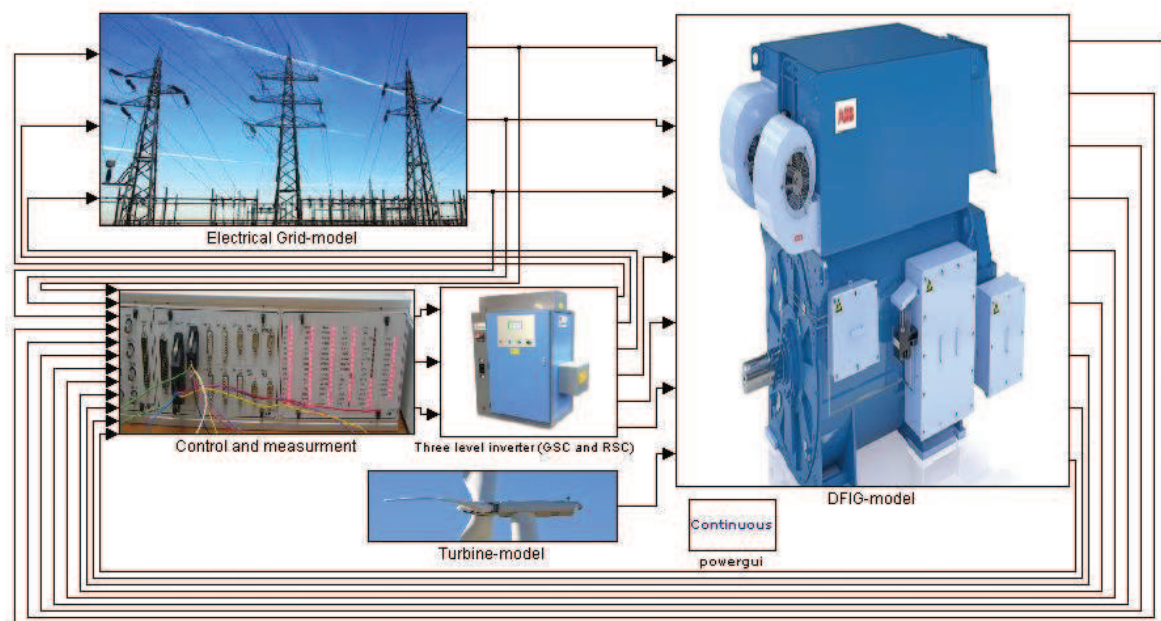


Figure 7. Simulink block diagram of the DFIG wind turbine model.

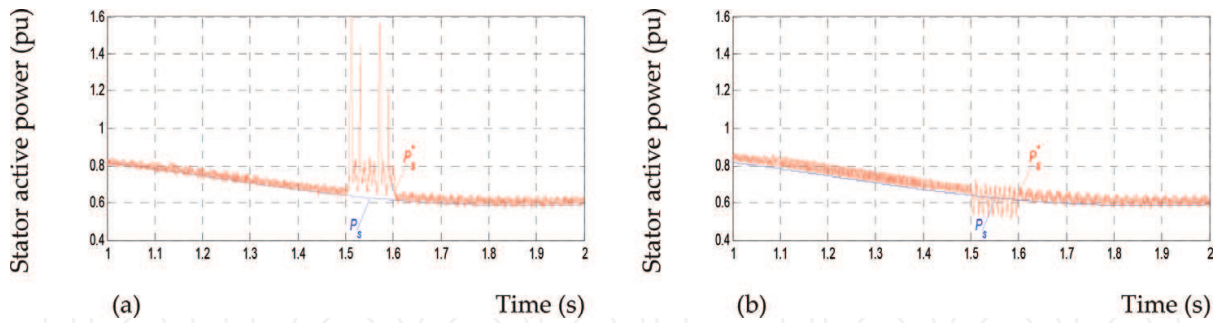


Figure 8. Stator active power (pu): (a) conventional single RCS, (b) proposed dual RCS.

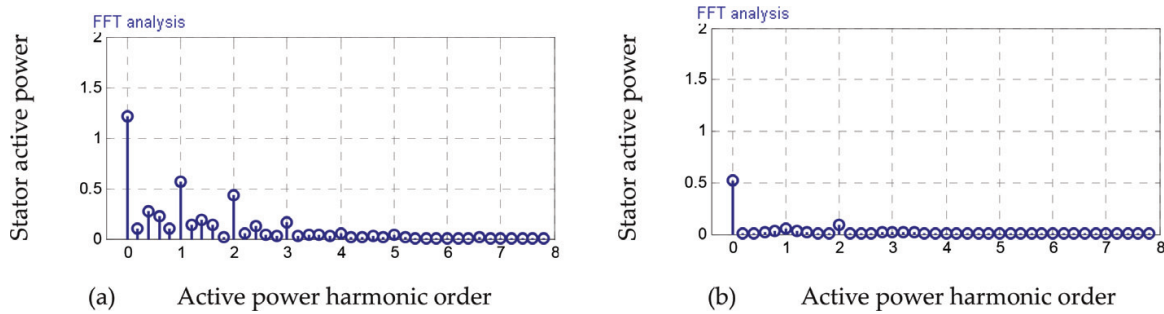


Figure 9. Harmonic spectra of the stator active power (pu): (a) conventional single RCS, (b) proposed dual RCS.

dual Lyapunov based robust control scheme (RCS), these results are compared with the conventional single Lyapunov-based RCS published in [15].

Figures 8(a) and (b), 9(a) and (b), 10(a) and (b) and 11(a) and (b), show that, during grid voltage unbalance, if conventional control is applied, the active and reactive powers contain important oscillations due to the nature of the second harmonic at twice the grid frequency (100 Hz) with magnitude of 0.78 pu. The conventional control does not provide adequate control of the negative sequence current during the occurrence or removal of voltage unbalance. Whereas, by using the proposed control method, these oscillations are dramatically reduced because of the negative sequence current compensation, during grid fault, by the dual current control loops which can indirectly control these powers.

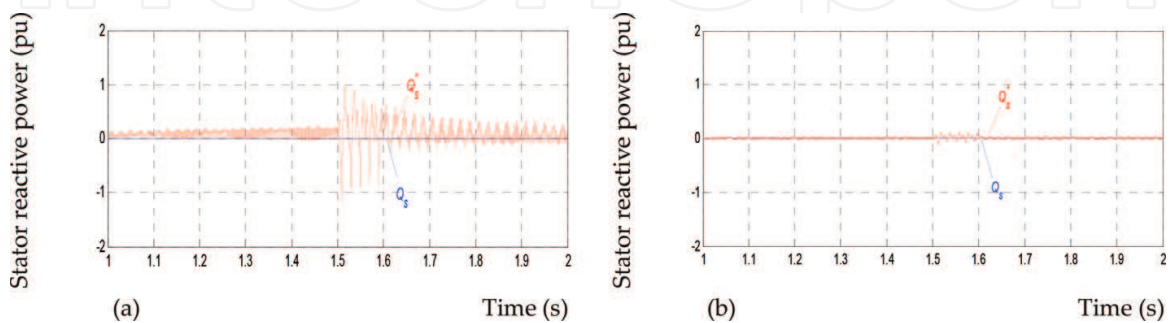


Figure 10. Stator reactive power (pu): (a) conventional single RCS, (b) proposed dual RCS.

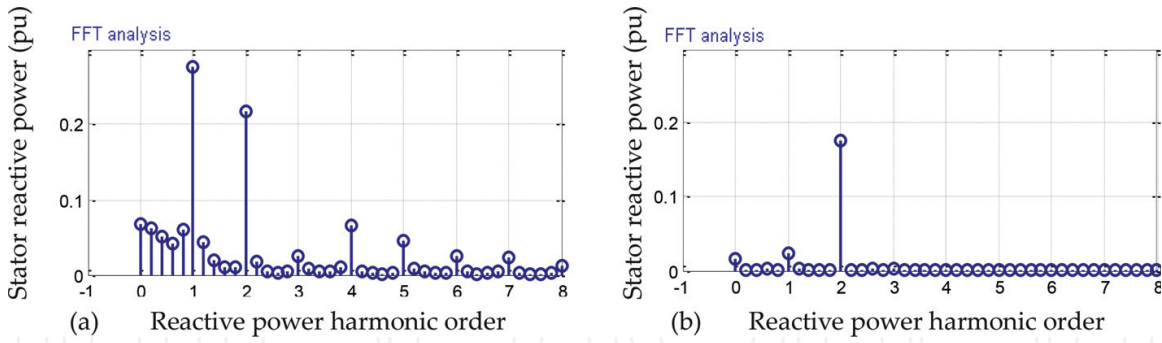


Figure 11. Harmonic spectra of the stator reactive power (pu): (a) conventional single RCS, (b) proposed dual RCS.

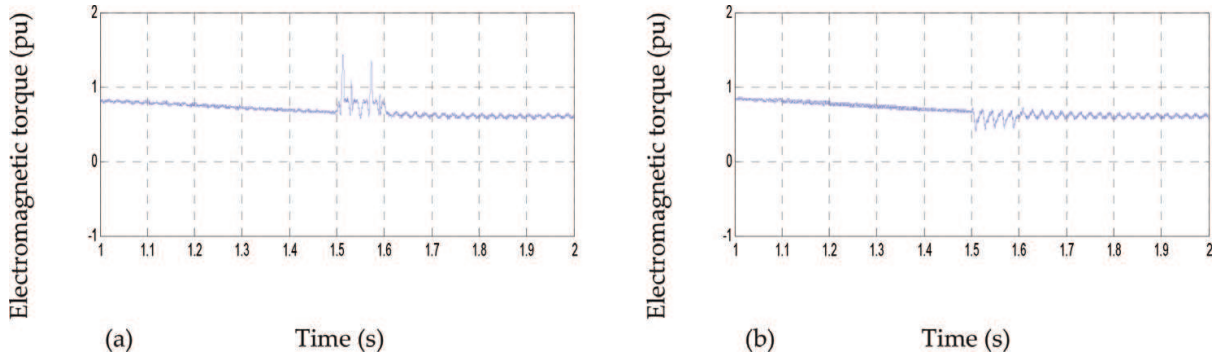


Figure 12. Electromagnetic torque (pu): (a) conventional single RCS, (b) proposed dual RCS.

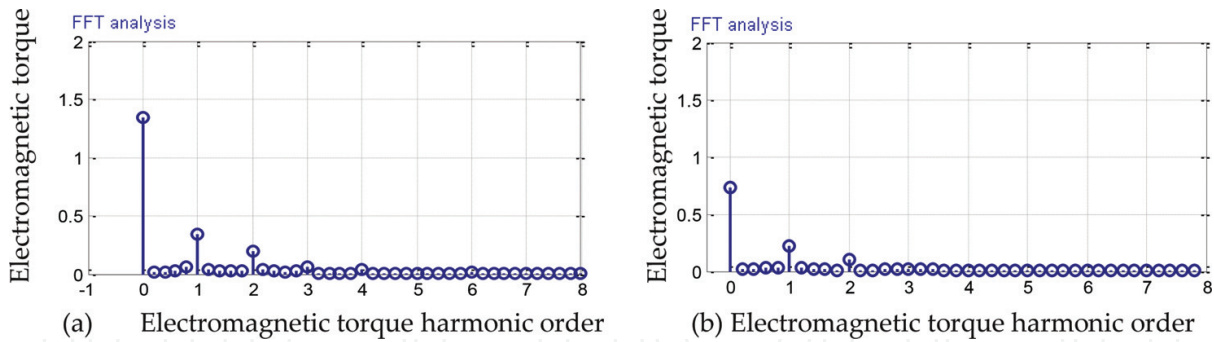


Figure 13. Harmonic spectra of the electromagnetic torque (pu): (a) conventional single RCS, (b) proposed dual RCS.

Figures 12(a) and (b) and 13(a) and (b) show that the ripples of the electromagnetic torque are also mitigated with the proposed control. On the contrary, when we use the conventional control method, the electromagnetic torque has oscillations with magnitude of 0.74 pu and frequency of 100 Hz, which might be harmful to the mechanical parts.

Figures 14(a) and (b) and 15(a) and (b) show that the stator currents have important harmonics with conventional control, which are injected into grid, but these currents are quite sinusoidal and symmetrical with the proposed control.

Figures 16(a) and (b) and 17(a) and (b) show that the currents at the rotor side are also unbalanced with conventional control, but these oscillations are attenuated by using the proposed

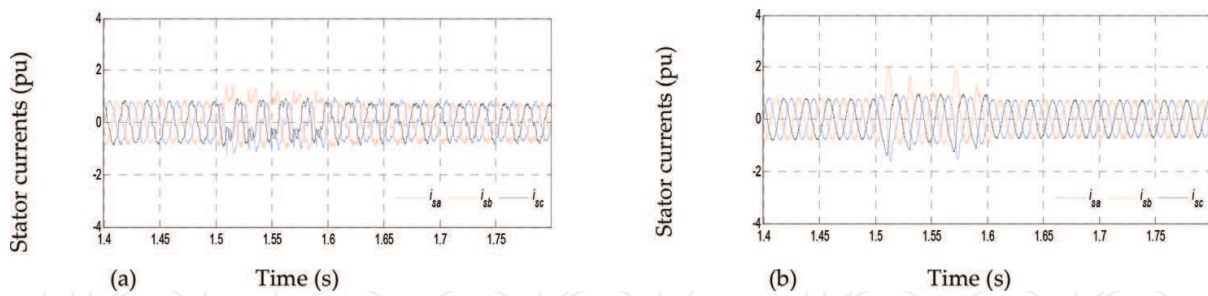


Figure 14. Stator currents (pu): (a) conventional single RCS, (b) proposed dual RCS.

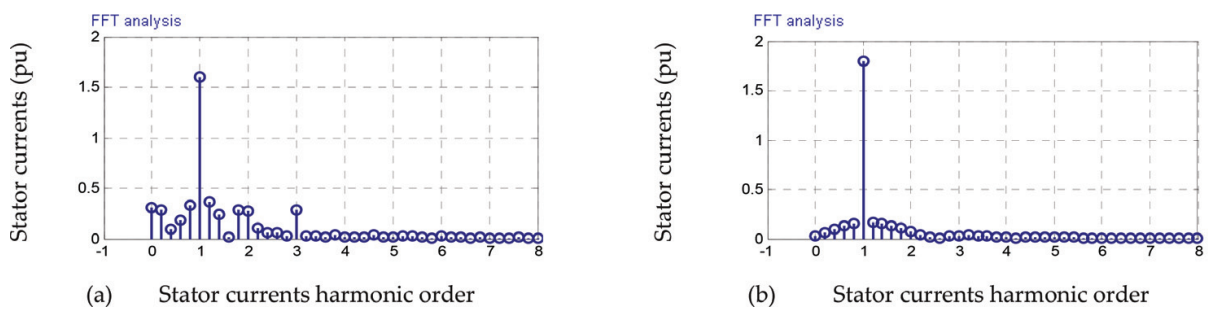


Figure 15. Harmonic spectra of the stator currents (pu): (a) conventional single RCS, (b) proposed dual RCS.

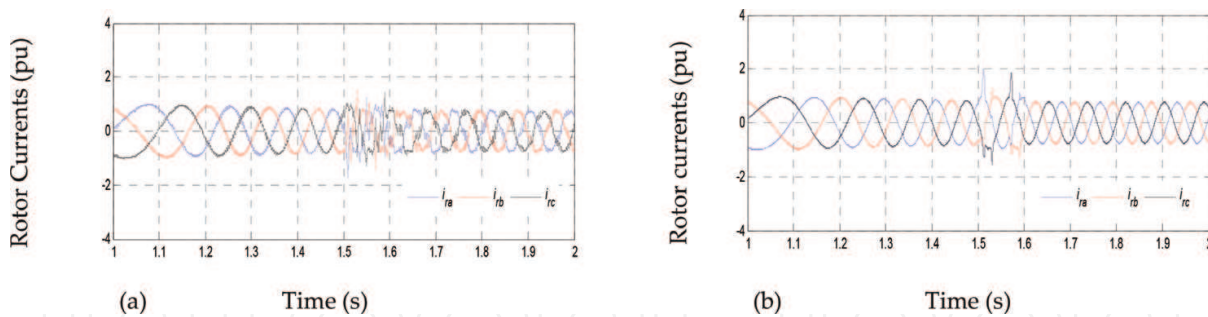


Figure 16. Rotor currents (pu): (a) conventional single RCS, (b) proposed RCS.

control method. This is due to the fact that the conventional control cannot control the negative component introduced by the unbalanced voltage in the stator flux and current vectors to zero. In that situation, interaction of these components in the generator develops motoring and generating behavior resulting in excessive oscillations. The stator flux amplitude is constant at the steady-state and rotates synchronously with the grid voltage. Instantly after the occurrence of the unbalanced voltage dip (see **Figure 3**), two voltages cause a positive and negative flux in the stator. Unlike the case of balanced voltage dip, where two components will be induced in the stator flux: the forced component is rotating with the grid frequency; afterward, the natural flux is static with the stator.

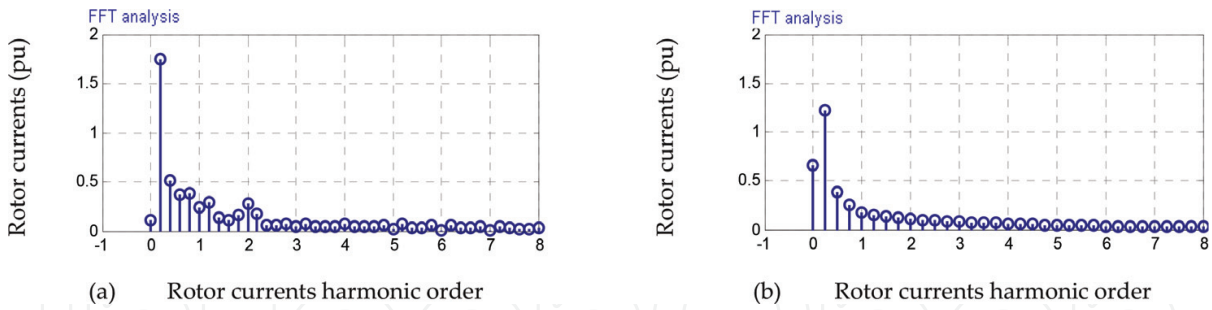


Figure 17. Harmonic spectra of the rotor currents (pu): (a) conventional single RCS, (b) proposed dual RCS.

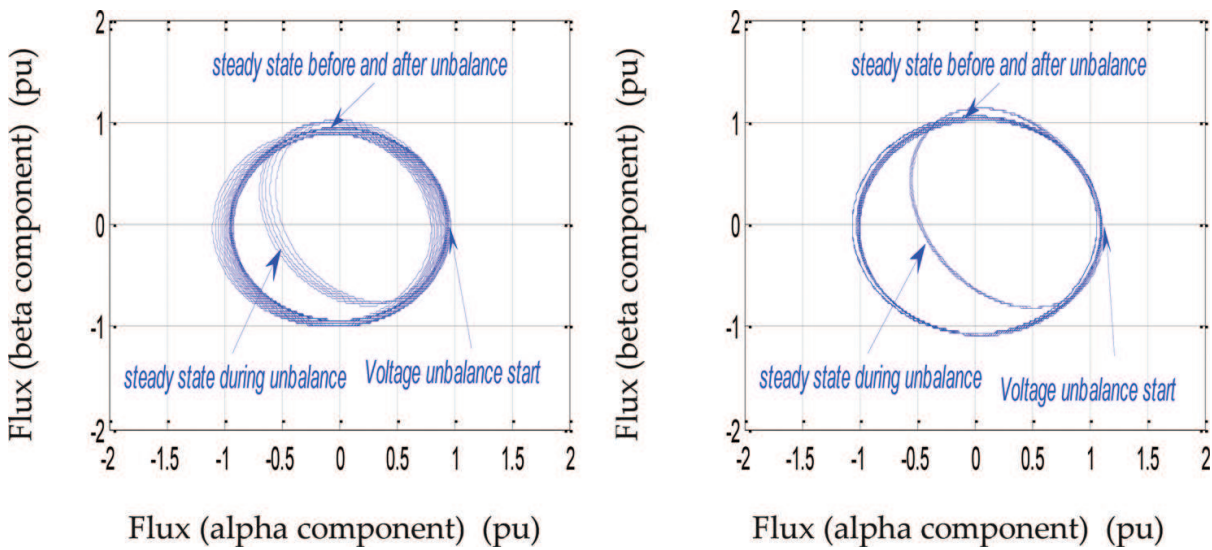


Figure 18. Stator flux (pu): (a) conventional single RCS, (b) proposed dual RCS.

Figure 18(a) and (b) shows the trajectory of the stator flux. Before the voltage unbalance, the stator flux traces a circle with radius equal to 1 pu. The flux of the stator with the proposed dual RCS is very well centered compared with that obtained with the conventional single RCS. When the voltage unbalance starts, the ellipse trajectory drawn by the flux is due to the presence of positive and negative flux in the stator rotating in opposite directions, which is a common characteristic in unbalanced voltage sags. Whereas, the natural flux brings the ellipse to be off-center. After the clearance of the voltage unbalance, the natural component of the stator flux is attenuated and the trajectory of the stator flux turns into the center again. However, it is noticed from these figures that compared with the proposed dual RCS, the stator flux trajectory of the conventional single RCS is not well centered with an important transient with a slow decay.

For clear illustrations, Figures 19 and 20 are included to show the comparative results of ripples pulsating at twice the grid frequency (100 Hz) in the stator active/reactive powers and electromagnetic torque among these different control strategies during network unbalance. As presented, the proposed dual RCS aims at mitigating the torque pulsations and the power

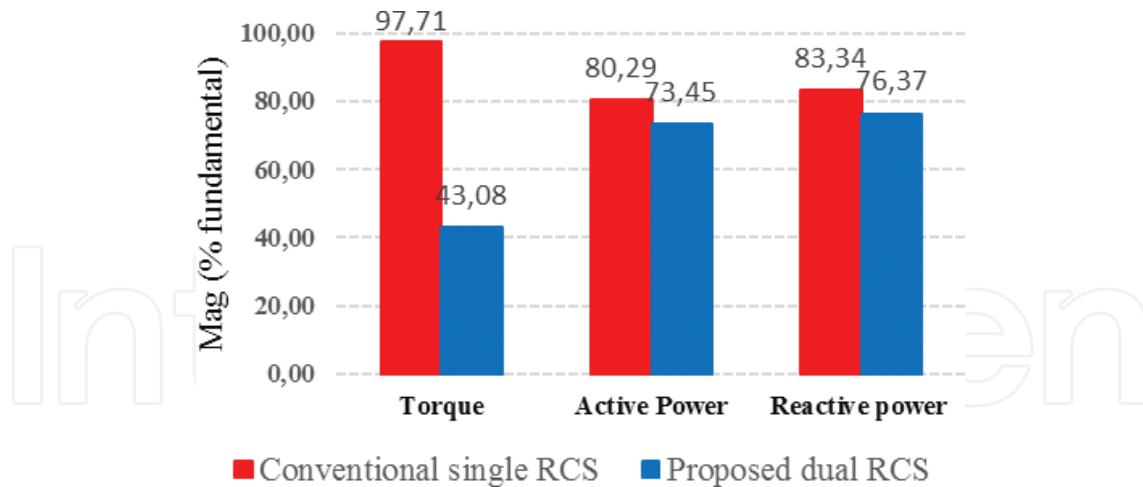


Figure 19. Comparison of ripples in electromagnetic torque, stator active and reactive power between the two control strategies.

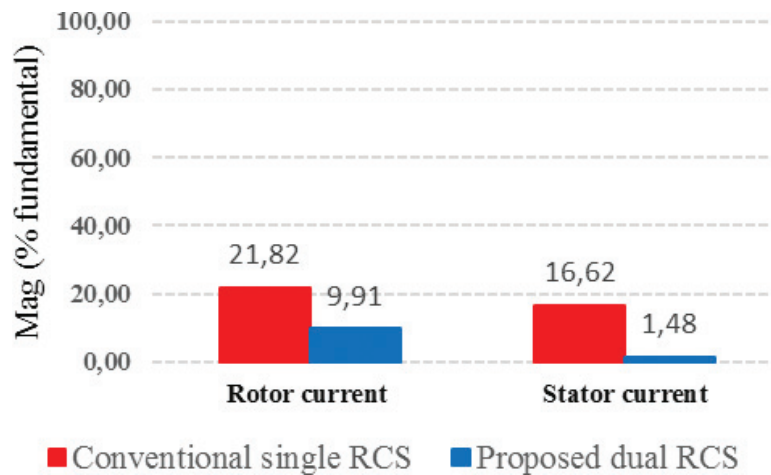


Figure 20. Comparison of harmonics in stator and rotor currents between the two control strategies.

ripples compared with the conventional method. In addition, the proposed dual RCS is able to reduce the harmonics of the rotor and stator currents. It can be concluded from these strategies that the proposed control method can effectively reduce the torque oscillations which incidentally may lead to a decrease of the fatigues on the turbine shaft.

5. Conclusions

In this chapter, an improved control strategy for doubly fed induction generator (DFIG)-based wind turbine under unbalanced grid voltage is presented. The dynamic behavior of DFIG by the proposed control algorithm proved to be suitable by a set of simulation tests using the MATLAB®/Simulink® environment. The results obtained imply that with the conventional single robust control scheme (RCS), the magnitude of the second harmonic oscillations can become high, intolerable and may lead to electrical and mechanical failure in function. After

removing the voltage unbalance, in the conventional control method, small oscillations appear in the powers and currents waveforms. On the contrary, when the proposed dual RCS is used, these power oscillations are effectively damped to a reasonable level. Furthermore, the proposed control strategy shows good performances and robustness by eliminating the pulsations in the torque which maybe preferred by wind farm operators since it will mitigate the fatigue of the turbine shaft as well as the gearbox. Moreover, symmetrical and sinusoidal stator and rotor currents are also obtained, in turn minimizing the copper losses in the rotor circuit, when the grid voltage is unbalanced. All computer simulations have been designed with a fixed-step size of 0.5 ms in order to consider digital implementation in future works.

A. Appendix

In this part, simulations are investigated with a 1.5 MW generator connected to a 690 V/50 Hz grid [15].

The generator's parameters are presented below:

Three pole pairs, $R_s = 0.012 \Omega$, $R_r = 0.021 \Omega$, $L_s = 0.0135 \text{ H}$, $L_r = +2.00372 \text{ e-4 H}$, $L_m = +1.7507 \text{ e-4 H}$,

Turbine's parameters: three blades, diameter = 70.5 m, gearbox ratio = 90: inertia (turbine + DFIG) = 1000 kg m² and viscous coefficient (turbine + DFIG) = 0.0024 kg m/s.

Author details

Kamel Djamel Eddine Kerrouche^{1*}, Lina Wang¹, Alex Van Den Bossche², Azzedine Draou³, Abdelkader Mezouar⁴ and Larbi Boumediene⁴

*Address all correspondence to: kerrouche20@yahoo.fr

1 School of Automation Science and Electrical Engineering, Beihang University, Beijing, China

2 Electrical Energy LAB EELAB, Ghent, Belgium

3 Department of Electrical Engineering, Islamic University of Madinah, Madinah, Saudi Arabia

4 Electro-technical Engineering Lab, Faculty of Technology, Tahar Moulay University, Saida, Algeria

References

- [1] Kerrouche K, Mezouar A, Belgacem K. Decoupled control of doubly fed induction generator by vector control for wind energy conversion system. *Energy Procedia*. 2013;**584**: 239-248

- [2] Gayen PK, Chatterjee D, Goswami SK. A low-voltage ride-through capability enhancement scheme of doubly fed induction generator based wind plant considering grid faults. *Journal of Renewable and Sustainable Energy*. 2016;**8**:025301
- [3] Kerrouche KDE, Mezouar A, Boumediene L, Kh B. Modeling and optimum power control based DFIG wind energy conversion system. *IREE*. 2014;**9**:174
- [4] Brekken TKA, Mohan N. Control of a doubly fed induction wind generator under unbalanced grid voltage conditions. *IEEE Transactions on Energy Conversion*. 2007;**22**:129
- [5] Mwasilu F, Justo JJ, Ro K-S, Jung J-W. Improvement of dynamic performance of doubly fed induction generator-based wind turbine power system under an unbalanced grid voltage condition. *IET Renewable Power Generation*. 2012;**6**:424
- [6] Abad G, Rodriguez MA, Iwanski G, Poza J. Direct power control of doubly fed induction generator based wind turbines under unbalanced grid voltage. *IEEE Transactions on Power Electronics*. 2010;**25**:442
- [7] Shehata EG. Active and reactive power control of doubly fed induction generators for wind energy generation under unbalanced grid voltage conditions. *Electric Power Components and Systems*. 2013;**41**:619
- [8] Hu J, Nian H, Hu B, He Y, Zhu ZQ. Direct active and reactive power regulation of DFIG using sliding mode control approach. *IEEE Transactions on Energy Conversion*. 2010;**25**:1028
- [9] Shang L, Hu J. Sliding-mode based direct power control of grid-connected wind-turbine-driven doubly fed induction generators under unbalanced grid voltage conditions. *IEEE Transactions on Energy Conversion*. 2012;**27**:362
- [10] Xu L, Wang Y. Dynamic modeling and control of DFIG-based wind turbines under unbalanced network conditions. *IEEE Transactions on Power Systems*. 2007;**22**:314
- [11] Lee S-B, Lee K-B, Lee D-C, Kim J-M. An improved control method for a DFIG in a wind turbine under an unbalanced grid voltage condition. *Journal of Electrical Engineering & Technology*. 2010;**5**:614
- [12] Norm's IEEE STD 519-1992: IEEE recommended practices and requirements for harmonic control in electrical power systems. April 12, 1993. pp. 15-99
- [13] Tedjini H, Meslem Y, Rahli M, Berbaoui B. Shunt active filter in damping harmonics propagation. *Advances in Electrical and Computer Engineering*. 2010;**10**:108-113
- [14] Abdou AF, Abu-Siada A, Pota HR. Improving the low voltage ride through of doubly fed induction generator during intermittent voltage source converter faults. *Journal of Renewable and Sustainable Energy*. 2013;**5**:043110
- [15] Kerrouche KDE, Mezouar A, Boumediene L, Van Den Bossche A. A comprehensive review of LVRT capability and sliding mode control of grid-connected wind-turbine-driven doubly fed induction generator. *Automatika—Journal for Control, Measurement, Electronics Computing and Communications*. 2016;**60**:922-935

- [16] Dash PK, Patnaik RK. Adaptive second order sliding mode control of doubly fed induction generator in wind energy conversion system. *Journal of Renewable and Sustainable Energy*. 2014;**6**:053143
- [17] Kerrouche K, Mezouar A, Boumediene L. A simple and efficient maximized power control of DFIG variable speed wind turbine. In: *Proceedings 3rd International Conference on Systems and Control (ICSC) IEEE, Algiers, Algeria*. 2013. p. 894
- [18] Kerrouche KDE, Mezouar A, Boumediene L, Van Den Bossche A. Modeling and Lyapunov-designed based on adaptive gain sliding mode control for wind turbines. *Journal of Power Technologies*. 2016;**96**:124

IntechOpen